THE JOURNAL OF BIOLOGICAL CHEMISTRY VOL. 286, NO. 23, pp. 20478–20489, June 10, 2011

Cortactin Is Required for N-cadherin Regulation of Kv1.5 Channel Function*[S]

Received for publication, January 4, 2011, and in revised form, April 19, 2011 Published, JBC Papers in Press, April 20, 2011, DOI 10.1074/jbc.M111.218560

Lan Cheng[‡], Aaron Yung[‡], Manuel Covarrubias[§], and Glenn L. Radice[‡1]

From the [‡]Center for Translational Medicine, Department of Medicine and the [§]Department of Neuroscience, Thomas Jefferson University, Philadelphia, Pennsylvania 19107

The intercalated disc serves as an organizing center for various cell surface components at the termini of the cardiomyocyte, thus ensuring proper mechanoelectrical coupling throughout the myocardium. The cell adhesion molecule, N-cadherin, is an essential component of the intercalated disc. Cardiac-specific deletion of N-cadherin leads to abnormal electrical conduction and sudden arrhythmic death in mice. The mechanisms linking the loss of N-cadherin in the heart and spontaneous malignant ventricular arrhythmias are poorly understood. To investigate whether ion channel remodeling contributes to arrhythmogenesis in N-cadherin conditional knock-out (N-cad CKO) mice, cardiac myocyte excitability and voltage-gated potassium channel (Kv), as well as inwardly rectifying K^+ channel remodeling, were investigated in N-cad CKO cardiomyocytes by whole cell patch clamp recordings. Action potential duration was prolonged in N-cad CKO ventricle myocytes compared with wild type. Relative to wild type, $I_{K,slow}$ density was significantly reduced consistent with decreased expression of Kv1.5 and Kv accessory protein, Kcne2, in the N-cad CKO myocytes. The decreased Kv1.5/Kcne2 expression correlated with disruption of the actin cytoskeleton and reduced cortactin at the sarcolemma. Biochemical experiments revealed that cortactin co-immunoprecipitates with Kv1.5. Finally, cortactin was required for N-cadherin-mediated enhancement of Kv1.5 channel activity in a heterologous expression system. Our results demonstrate a novel mechanistic link among the cell adhesion molecule, N-cadherin, the actin-binding scaffold protein, cortactin, and Kv channel remodeling in the heart. These data suggest that in addition to gap junction remodeling, aberrant Kv1.5 channel function contributes to the arrhythmogenic phenotype in N-cad CKO mice.

The cellular activity of both excitable and nonexcitable cells depends on the coordinated activities of membrane ion channels, transporters, pumps, receptors, scaffold, and cytoskeleton (1, 2). A high resolution image of the site of end-end contact between cardiomyocytes reveals an electron-dense organization called the intercalated disc (ICD).[2] Its classic definition involves three structures: adherens junctions and desmosomes, providing mechanical coupling; and gap junctions, providing electrical coupling (3, 4). N-cadherin is the primary cell adhesion molecule responsible for maintaining the ICD structure as it interacts intracellularly with catenins, which mediate linkage to the actin cytoskeleton (5, 6). We previously reported that cardiac-specific loss of N-cadherin leads to disassembly of the ICD and spontaneous lethal ventricular tachyarrhythmias (7, 8).

Ventricular tachyarrhythmias are a frequent cause of sudden cardiac death in ischemic and nonischemic heart disease (9). Despite intense investigation, molecular mechanisms underlying the propensity of diseased myocardium to initiate and propagate lethal arrhythmias are incompletely understood. In recent years, a number of genetically engineered murine models have been developed to explore the pathophysiology of arrhythmogenesis. Although many such mice display increases in the frequency of spontaneous or inducible ventricular ectopy, in almost all cases this activity is self-limited and has not been shown to be the proximate cause of death. Several other mutant mouse models are able to support sustained ventricular arrhythmias (10), but these require provocative stimuli, such as exercise with administration of adrenergic agents. To date, only the heart-specific connexin43 (Cx43) (11), vinculin (12), and N-cadherin (7) knock-out mice have been shown to die prematurely from spontaneous sustained ventricular tachyarrhythmias. Because of the arrhythmic propensity of the N-cad CKO mice and the ease of inducible sustained arrhythmias, it has served as a model for the study of basic mechanisms of arrhythmia.

In N-cad CKO myopathic hearts, there is a significant reduction in Cx43-containing gap junctions causing decreased ventricular conduction velocity (8). Abnormal expression of Cx43 (gap junction remodeling) may contribute directly to the arrhythmic substrate. However, the severity of gap junction remodeling, in terms of the extent of connexin mislocalization away from the intercalated disc as well as the overall diminution of expression, can be highly variable. Thus, it remains uncertain whether only the down-regulated Cx43 expression in the N-cad CKO heart relates to the likelihood of arrhythmogenesis. We hypothesized that uncoupling promotes regional

* This work was supported, in whole or in part, by National Institutes of Health Grant HL081569 (to G. L. R.). This work was also supported in part by National Institutes of Health Cancer Center Core Grant 5 P30 CA-56036 (to the Kimmel Cancer Center) and American Heart Association Established Investigator Grant 0440114N (to G. L. R.).

[S] The on-line version of this article (available at http://www.jbc.org) contains supplemental Tables S1 and S2 and Figs. S1–S5.

[1] To whom correspondence should be addressed: Thomas Jefferson University, Rm. 309 College Bldg., 1025 Walnut St., Philadelphia, PA 19107. Fax: 215-503-5731; E-mail: glenn.radice@jefferson.edu.

[2] The abbreviations used are: ICD, intercalated disc; N-cad CKO, N-cadherin conditional knock-out; APD, action potential duration; KChIP, Kv channel interacting protein; Kir, inwardly rectifying; I_{K1}, inwardly rectifying K^+ currents; Tam, tamoxifen; HP, holding potential; bis-tris, 2-[bis(2-hydroxyethyl)amino]-2-(hydroxymethyl)propane-1,3-diol; TfR, transferrin receptor.

ion channel remodeling, thereby increasing electrical heterogeneity and facilitating the development of arrhythmia. Accordingly, to explore this possibility, we studied cardiac excitability and ion channel remodeling in N-cad CKO hearts in which N-cadherin expression decreases progressively throughout the ventricular myocardium post tamoxifen administration. Here we demonstrate that a loss of N-cadherin contributes to the incidence of arrhythmias not only through conduction slowing but also through significant remodeling of the major outward potassium currents. Finally, we show a novel mechanistic link among the cell adhesion molecule, N-cadherin, the actin-binding scaffold protein, cortactin, and Kv channel remodeling in the heart.

EXPERIMENTAL PROCEDURES

Generation of N-cadherin-deficient Cardiomyocytes—The N-cad CKO mice have been described previously (7). In brief, cardiac-specific Cre recombinase, α-myosin heavy chain-MerCreMer, N-cadherin flox/flox mice were mated with N-cadherin flox/flox mice. N-cadherin floxed mice with or without the Cre transgene (6–10 weeks old) were administered tamoxifen (Tam; Sigma) by intraperitoneal injection once a day for 5 days at a dosage of 80 mg/kg mice. By 5 weeks post Tam, N-cad CKO mice begin to exhibit sudden arrhythmic death (8). Therefore, electrophysiological and immunofluorescence experiments were performed on cardiomyocytes isolated from N-cad CKO mice 5–6 weeks post Tam. The N-cad CKO mice were analyzed in a mixed 129Sv/C57Bl/6J genetic background, and littermates were used as controls. All of the animal procedures and experiments were performed in accordance with the guidelines of the institutional animal care and use committee of Thomas Jefferson University.

Electrophysiological Recordings—Cardiomyocytes were isolated from adult hearts as described previously (13). The whole cell patch clamp recordings were obtained from myocytes isolated from the left ventricles of adult (3–4 month old) WT (n = 12) and N-cad CKO (n = 8) mouse hearts. Electrophysiological experiments were conducted using an Axopatch 200A amplifier (Molecular Devices, Union City, CA), interfaced to a Dell microcomputer with a Digidata 1322A series analog/digital interface (Molecular Devices), using pClamp 8 software (Molecular Devices). Whole cell patch clamp experiments were conducted at room temperature (22–24 °C). Recording pipettes contained 135 mmol/liter KCl, 1 mmol/liter $MgCl_2$, 10 mmol/liter EGTA, 10 mmol/liter HEPES, and 5 mmol/liter glucose (pH 7.2; 310 mOsm). The bath solution contained 136 mmol/liter NaCl, 4 mmol/liter KCl, 1 mmol/liter $CaCl_2$, 2 mmol/liter $MgCl_2$, 5 mmol/liter $CoCl_2$, 10 mmol/liter HEPES, 0.04 mmol/liter tetrodotoxin, and 10 mmol/liter glucose (pH 7.4; 300 mOsm). For current clamp experiments, the tetrodotoxin and $CoCl_2$ were omitted from the bath. Patch electrodes were fabricated and polished by heating. We used pipettes with resistance of 2–4 MΩ. Whole cell membrane capacitances and series resistances were compensated electronically prior to recording voltage clamp currents. Voltage errors resulting from the uncompensated series resistance were always ≤8mV and were not corrected. The experimental data were sampled at 5 kHz; current and voltage signals were low pass-filtered at 1 kHz prior to digitization and storage. For current clamp experiments, a series of 1-ms-long current steps from 10 to 250 pA in 20-pA increments were delivered at 1-Hz frequency to cells in each group.

Depolarization-activated outward K^+ (Kv) currents were recorded in response to 4.5-s voltage steps to potentials between −40 and +40 mV from a holding potential (HP) of −70 mV; voltage steps were presented in 10-mV increments at 15-s intervals. Inwardly rectifying K^+ currents, I_{K1}, were recorded in response to 350-ms voltage steps to test potentials between −40 and −120 mV (in 10-mV increments) from the same HP.

For current clamp analyses, the numeric value (action potential threshold, width, etc.) was taken from the first action potential initiated on current injection. Action potential threshold were determined from phase plane plot (14). Resting membrane potentials, action potential amplitudes, and action potential durations at 25% (APD_{25}), 50% (APD_{50}), 75% (APD_{75}), and 90% (APD_{90}) repolarization were measured using Clampfit (Molecular Devices). Voltage clamp data were compiled and analyzed using Clampfit and Origin 7.0 (OriginLab Corp., Northampton, MA) software. Whole cell membrane capacitances (C_m) were acquired from Clampex (Molecular Devices). Leak currents were always <10 pA and were not corrected. Peak Kv currents at each test potential were defined as the maximal outward K^+ current recorded during the 4.5-s voltage steps. The decay phases of the outward K^+ currents evoked during 4.5-s depolarizing voltage steps are described by the sum of two exponentials: $y(t) = A_1\exp(-t/\tau_1) + A_2\exp(-t/\tau_2) + B$, where t is time, τ_1 and τ_2 are the decay time constants, A_1 and A_2 are the amplitudes of the inactivating current components ($I_{to,fast}$ or $I_{to,f}$ and $I_{K,slow}$), and B is the amplitude of the noninactivating current component, I_{ss}. Fitting residuals and correlation co-efficients were determined to assess the quality of fits; only fits with correlation co-efficients >0.980 were used in this study (supplemental Fig. S1). In all cells, I_{K1} densities were determined from the amplitudes of the currents measured at the end of 350-ms hyperpolarizing voltage steps (−90 to −120 mV) from a HP of −70 mV. Current amplitudes in each cell were normalized to whole cell membrane capacitances (in the same cell), and current densities (pA/pF) are reported.

Quantitative RT-PCR—RNA was extracted from ventricles using TRIzol reagent (Invitrogen), DNase-cleaned, and reverse transcribed using the iScript cDNA synthesis kit (Bio-Rad), and PCR was performed with iQ SYBR Green Supermix (Bio-Rad) in the MyiQ single-color real time PCR detection system (Bio-Rad). Results for each sample were normalized to GAPDH and expressed according to the $2^{-\Delta C_t}$ method (15), as relative mRNA expression compared with GAPDH. The following primers were used for real time PCR (5′ to 3′): Kv1.5, CCTGCGAAGGTCTCTGTATGC (sense) and TGCCTCGATCTCTCTTTACAAATCT (antisense); KCNE2, CACATTAGCCAATTTGACCCAGA (sense) and GAACATGCCGATCATCACCAT (antisense); Kv4.2, GCCGCAGCACCTAGTCGTT (sense) and CACCACGTCGATGATACTCATGA (antisense); and GAPDH, CACTCTTCCACCTTCGATG (sense) and TCCACCACCCTGTTGCTGTA (antisense).

Western Blot Analysis—To enrich for ion channels, crude ventricular membrane fractions were prepared similar to described previously (16). Western blot analyses were performed on fractionated ventricular membrane proteins prepared from adult WT and N-cad CKO hearts. Briefly, the hearts were homogenized in buffer consisting of (in mmol/liter) 25 Tris-HCl, pH 7.5, 5 EDTA, pH 8, 5 EGTA, pH 8. Nuclei and debris were pelleted by centrifugation at 1,000 × *g* for 10 min. This procedure was repeated, and the supernatants from both low speed spins were pooled and centrifuged at 80,000 × *g* for 30 min. The pellets were resuspended in the above solution and centrifuged at 80,000 g for another 10 min. The final pellets were sonicated and solubilized in radioimmune precipitation assay buffer consisting of 50 mmol/liter Tris-HCl, pH 7.5, 5 mmol/liter EDTA, pH 8, 150 mmol/liter NaCl, 0.1% SDS, 1% Nonidet P-40, and 0.5% sodium deoxycholate for 1 h. Insoluble material was centrifuged at 13,000 rpm for 10 min. Solubilized membranes were aliquoted and stored frozen at −80 °C until used. The protein content of each of the solubilized membrane preparations was determined using a protein assay kit (Thermo Scientific, Rockford, IL). The proteins were separated on a NuPAGE-Novex 4–12% bis-tris gel (Invitrogen) and transferred onto nitrocellulose membranes. The membranes were then blocked and incubated overnight at 4 °C with primary antibodies. The membranes were probed with polyclonal anti-kcne2 antibody (Sigma); Kv1.5 and Kv4.2 (Alomone, Jerusalem, Israel); Kv2.1, Kv4.3, KChIP2, Kvβ1.1, and Kvβ2 (University of California, Davis NINDS/NIMH NeuroMab Facility, Davis, CA); and transferrin receptor (TfR) antibody (Zymed Laboratories Inc.) overnight at 4 °C. The proteins were visualized with a LI-COR infrared imager (Odyssey). Quantitative densitometric analysis was performed using Odyssey version 1.2 infrared imaging software.

Immunofluorescence—Double immunofluorescence detection of Kv channel pore forming subunits (Kv4.2, Kv4.3, Kv1.5, Kv1.4, and Kv2.1), auxiliary subunits (kcne2, KChIP2, Kvβ1, and Kvβ2), and actin cytoskeleton or cortactin was performed as described previously (17). Briefly, freshly isolated myocytes were fixed in 4% paraformaldehyde for 20 min and subsequently suspended in PBS for immunostaining. The cells were collected from 3 to 6 animals for each group. The cells were permeabilized and blocked with 0.2% Triton X-100 (Sigma) and 5% goat serum (Invitrogen) in PBS and then incubated in primary antibody overnight at 4 °C. The following primary antibodies were used: rabbit Kv1.5 (1:10; Alomone Labs), mouse Kv2.1 (1:10; NeuroMab), mouse Kv4.2 (1:10; NeuroMab), mouse Kv4.3 (1:10; NeuroMab), mouse Kv1.4 (1:10; NeuroMab), mouse KChIP2 (1:10; NeuroMab), rabbit kcne2 (1:200; Sigma), mouse Kvβ1 (1:10; NeuroMab), mouse Kvβ2 (1:10; NeuroMab), mouse Kir2.1 (1:50; NeuroMab), mouse Kir2.2 (1:50; NeuroMab), sarcomeric α-actinin (1:200, EA-53; Sigma), mouse N-cadherin (1:200; Invitrogen), mouse α-actin (1:200, cardiac clone AC1–20.4.2; Sigma), rabbit actin (1:200, clone SIG2-AC2; Sigma), and mouse cortactin (1:200; Millipore). After washes with 0.1% Tween 20 in PBS, the cells were incubated with goat anti-mouse Cy3 (Jackson ImmunoResearch Laboratories), goat anti-mouse Alexa Fluor 488 (Molecular Probes), goat anti-rabbit Alexa Fluor 555 (Molecular Probes), or goat anti-rabbit Alexa Fluor 488 (Invitrogen) secondary antibodies for 1 h at room temperature and mounted using ProLong® Gold antifade reagents (Invitrogen). Stained slides were viewed with a Zeiss LMS510 Meta confocal microscope. All of the confocal images represent a single optical slice through the middle of the cell.

To quantitatively assess Kv-channel distribution in myocytes, eight Z-scan images were obtained at 0.25-μm intervals from middle of each cell. As described previously (18), pixel intensities at the cell periphery of cardiomyocytes from eight optical slices were determined using the histogram function in National Institutes of Health ImageJ software v1.42.

Immunoprecipitation—HEK-293 cells were transiently transfected with a plasmid encoding Kv1.5-eGFP fusion protein (kindly provided by Jeanne Nerbonne, Washington University Medical School, St. Louis, MO) or GFP alone. HEK-293 cells and adult mouse ventricular tissue samples were harvested, quickly frozen, and stored at −80 °C. Cortactin-enriched fractions were prepared for immunoprecipitation, according to a previously described method (19). Briefly, the samples were lysed in 1 ml of Triton lysis buffer (100 mM KCl, 1 mM 1,2-Bis(2-Aminophenoxy)ethane-*N*,*N*,*N*′,*N*′-tetraacetic acid (BAPTA), 1 mM sodium orthovanadate, 1 mM dithiothreitol, 20 mM HEPES, 0.5% Triton X-100, protease inhibitors, pH 7.4, at 4 °C). The lysate was transferred to a 1.5-ml microcentrifuge tube and centrifuged at 20,000 × *g* for 4 min. The supernatant was transferred to an ultracentrifuge tube and centrifuged at 100,000 × *g* for 1 h. The soluble fraction supernatant was transferred to a fresh microcentrifuge tube. The remaining high speed pellet was washed and resuspended in a modified radioimmune precipitation assay buffer (50 mM Tris, 150 mM NaCl, 1 mM EDTA, 1% Nonidet P-40, 0.25% deoxycholate, 0.1% SDS, 10% glycerol, 1 mM dithiothreitol, 1 mM NaF, 1 mM sodium orthovanadate, and protease inhibitors, pH 7.4 at 4 °C). Rabbit polyclonal anti-cortactin and monoclonal anti-GFP antibodies were from Santa Cruz Biotechnology, Inc. (Santa Cruz, CA). Rabbit polyclonal anti-Arp2 (actin-related protein 2) antibodies were from Cell Signaling Technology, Inc. (Danvers, MA).

Oocyte Experiment—The human N-cadherin, human Kv1.5, Kv4.2, and rat Kv2.1 clones were kind gifts from Dr. Guiscard Seebohm (Ruhr University Bochum, Bochum, Germany). For co-expression experiments, Kv channels and N-cadherin cRNA were diluted into the same concentrations, and oocytes were injected with equal volume of cRNA between Kv channels and N-cadherin. For antisense DNA oligonucleotides, the oocytes were injected with 120 ng of HPLC-purified antisense DNA oligonucleotide (Integrated DNA Technologies) directed against *Xenopus* cortactin: C*A*G*T*CGTCTGTCTCA*T*-C*T*G (where the asterisks indicate phosphorothioated bases) immediately after injection of 1.5 ng of Kv1.5 cRNA 48 h before recording, as previously shown (20). Scrambled control oligonucleotides were injected as negative control at the same recording condition and on the same batch of oocytes. To harvest oocytes, *Xenopus laevis* frogs were handled according to a protocol approved by the institutional animal care and use committee of Thomas Jefferson University. For expression in oocytes, cRNA was synthesized *in vitro* as described previously (21). 1–3 days after the injection of the cRNA into defolliculated

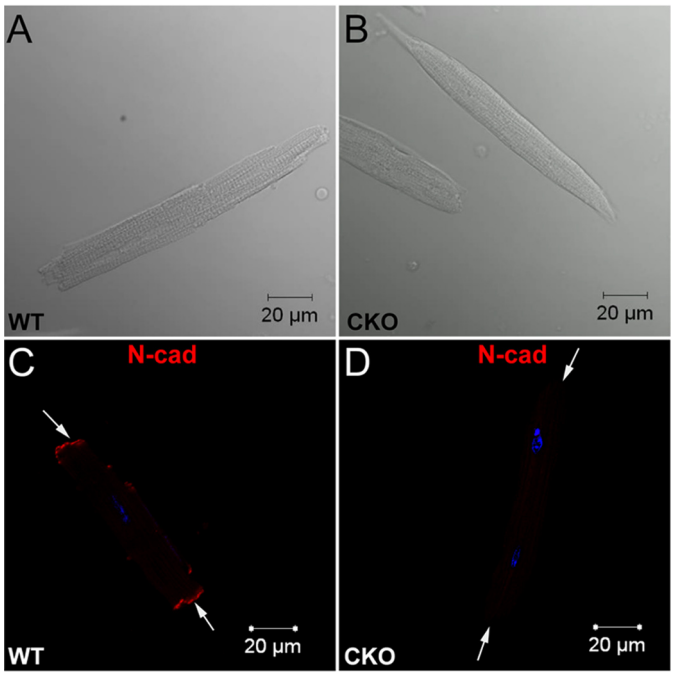

FIGURE 1. **Altered morphology of N-cadherin-deficient cardiomyocytes.** *A* and *B*, brightfield images of isolated adult ventricular myocytes from WT (*A*) and N-cad CKO (*B*) mice. *C* and *D*, immunostaining for N-cadherin showed the expected loss of N-cadherin from the ICD in the N-cad CKO (*D*) compared with WT (*C*) myocyte. The nuclei are stained with DAPI (*blue*). The *arrows* indicate the termini of the cells.

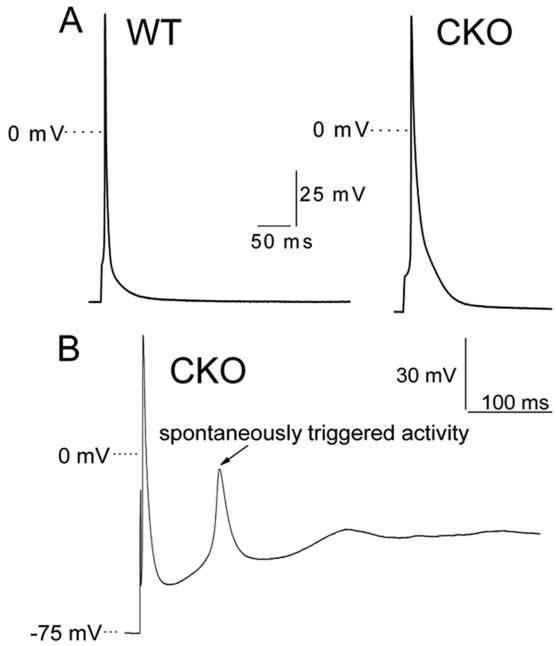

FIGURE 2. **Action potential waveforms in WT and N-cadherin CKO ventricular myocytes were distinguishable.** *A*, representative action potential waveforms, recorded from isolated WT (*left trace*) and N-cad CKO (*right trace*) ventricular myocytes are illustrated. *B*, spontaneously triggered activity was observed in N-cad CKO (3 of 14) but not WT (0 of 12) ventricular myocytes ($\chi^2 = 7.69$, $p < 0.05$).

oocytes, the two-electrode voltage clamp method was used to record the expressed whole oocyte currents in normal extracellular bath solution (ND96) according to established procedures (22). Details of the voltage clamp protocols are described in the figure legends. The results are expressed as the means ± S.E. Statistical significance was examined with Student's *t* test, one-way analysis of variance or chi-squared test. $p < 0.05$ was considered significant.

RESULTS

Action Potential Durations Are Prolonged in N-cad CKO Animals—Given the propensity of the cardiac-specific N-cadherin knock-out mice to develop spontaneous lethal ventricular tachycardia (7, 8), we hypothesized that in addition to conduction slowing, the loss of N-cadherin may contribute to arrhythmogenesis by altering ion channel function, thus increasing electrical heterogeneity. To investigate this possibility, ventricular myocytes were isolated from α-myosin heavy chain/MerCreMer, N-cad$^{flox/flox}$ (N-cad CKO), and N-cad$^{flox/flox}$ without Cre (WT) adult mice 5 weeks post Tam. WT myocytes showed their characteristic rod shape and the existence of N-cadherin at ICD (Fig. 1, *A* and *C*). However, N-cadherin-deficient cardiomyocytes no longer displayed the characteristic interdigitating or step-like structures at the termini representing the ICD consistent with our previous ultrastructural analysis, demonstrating disassembly of the ICD in N-cad CKO myocardium (7). The loss of N-cadherin resulted in spindle shaped myocytes (Fig. 1, *B* and *D*). To determine whether electrical excitability was altered in the absence of N-cadherin, action potential recordings were conducted on isolated left ventricular myocytes. Current clamp experiments revealed that action potentials recorded from N-cad CKO myocytes were substantially broader than action potentials recorded from cells isolated from WT littermates, with the latter phase of repolarization being particularly affected (Fig. 2*A*). Measurements of action potential durations at 25, 50, 75, and 90% repolarization (APD_{25}, APD_{50}, APD_{75}, and APD_{90}) revealed that mean action potential durations at 75 and 90% repolarization times were prolonged significantly compared with action potential durations in WT myocytes (Fig. 2*A* and supplemental Table S1). Mean ± S.E. APD_{75} and APD_{90} for example, were 9.1 ± 0.5 and 26.5 ± 2.3 ms ($n = 12$) in WT cells and 17.9 ± 2.8 and 63.5 ± 10.9 ms ($n = 11$) in N-cad CKO cells (supplemental Table S1). In accordance with the increased arrhythmia susceptibility in N-cad CKO mice (7), spontaneously triggered activity, presumably resulting from early after depolarizations, was only observed in N-cad CKO ventricular cells (3 of 14 in CKO group *versus* 0 of 12 in WT ($\chi^2 = 7.69$, $p < 0.05$) (Fig. 2*B*). However, the input resistance, threshold currents to evoke action potential of ventricular myocytes from WT and N-cad CKO animals were indistinguishable.

Outward K^+ Currents Are Attenuated in N-cad CKO Ventricular Myocytes—Kv channels play key roles in determining the amplitudes and the durations of action potentials in mouse cardiac cells (23). Previous studies have documented five major kinetically and pharmacologically distinct Kv channels in adult mouse ventricular myocytes (24, 25): (*a*) a rapidly activating and inactivating, "fast transient" K^+ current, Kv4.2 subunits underlie $I_{to,f}$; (*b*) a rapidly activating, slowly inactivating, "slow transient" current, Kv1.4 subunits underlie $I_{to,s}$; (*c*) a rapidly activating, very slowly inactivating current, Kv1.5 subunits underlie $I_{K,slow1}$, Kv2.1 subunits underlie $I_{K,slow2}$; (*d*) a slowly activating, noninactivating current, Kv2P α subunits underlie

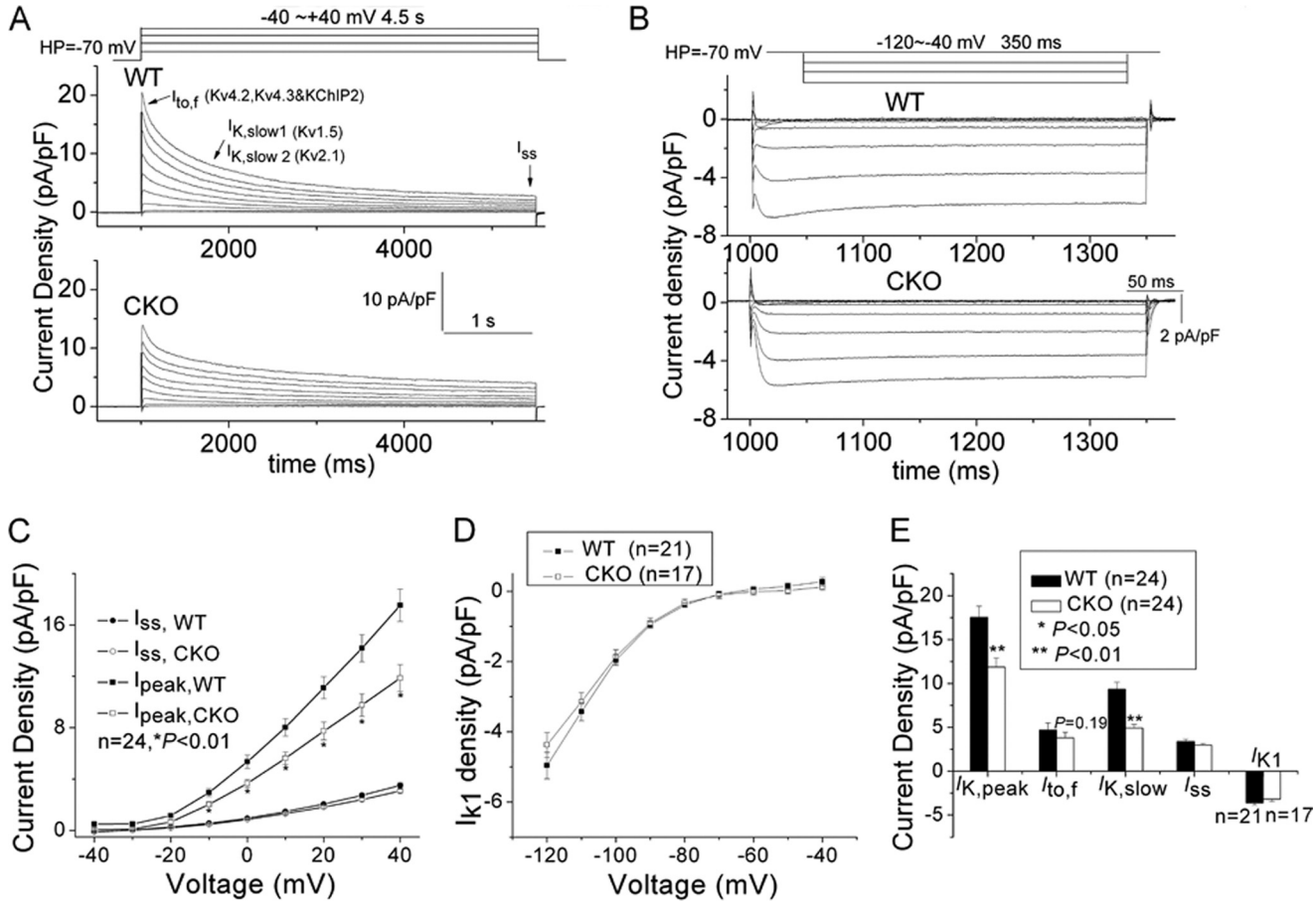

FIGURE 3. **Outward K^+ current waveforms were altered in N-cadherin CKO cardiomyocytes.** Whole cell outward K^+ currents, recorded from ventricular myocytes isolated from adult WT and N-cad CKO littermates, were evoked during 4.5-s depolarizing voltage steps to potentials between −40 and +40 mV from a HP of −70 mV. *A*, the waveforms of the Ca^{2+}-independent, depolarization-activated outward K^+ currents in WT and CKO cardiomyocytes were distinct. *B*, representative whole cell I_{K1} currents between −40 and −120 mV (HP = −70 mV) in WT and CKO ventricular cells. There was no apparent change in WT and CKO ventricular cell. *C*, peak outward K^+ current densities at all of the voltages were reduced in the N-cad CKO group, whereas I_{ss} densities are not significantly different. *D*, no change in inward I_{K1} current densities at all the voltages in CKO group. *E*, the slowly decaying current components ($I_{K,slow}$) were much less prominent in CKO cells compared with the currents recorded from the WT cell. The decay phases of the outward K^+ currents in records such as those in *A* were analyzed to provide the amplitudes of $I_{to,f}$, $I_{K,slow}$, I_{ss}, and I_{K1} in individual cells and normalized to the whole cell membrane capacitance (determined in the same cell).

I_{ss}; and (*e*) an inwardly rectifying potassium current, Kir2.1, Kir2.2 subunits underlie I_{K1}. To determine whether *N-cadherin* deletion affects repolarizing voltage-gated K^+ (Kv) currents, whole cell Kv currents were recorded from ventricular myocytes isolated from N-cad CKO and WT littermates. With voltage-gated Ca^{2+} and Na^+ currents blocked, outward currents were routinely recorded during 4.5-s depolarizing voltage steps to potentials between −40 and +40 mV from a holding potential of −70 mV. Representative outward K^+ current waveforms recorded in WT and N-cad CKO adult mouse ventricular myocytes are illustrated in Fig. 3*A*. In both cell types, the rates of rise and the amplitudes of the currents increase with increasing depolarization; the largest and most rapidly activating current in Fig. 3*A* was evoked at +40 mV. The currents recorded and analyzed here, therefore, are assumed to reflect only the activation of Ca^{2+}-independent, depolarization-activated K^+ channels. Whole cell voltage clamp recordings revealed that the waveforms of the depolarization-activated outward K^+ currents in ventricular myocytes isolated from N-cad CKO and WT littermates are distinct (Fig. 3*A*). As illustrated in Fig. 3*C*, peak outward K^+ current densities at all test potentials are lower in cells isolated from N-cad CKO animals compared with the currents typically recorded in myocytes isolated from WT littermates. Quantitative analyses confirmed that the means ± S.E. I_{peak} densities at +40 mV in N-cad CKO (11.8 ± 1.0 pA/pF; $n = 24$) and WT (17.5 ± 1.3 pA/pF; $n = 24$) ventricular myocytes were significantly different (Fig. 3*C*). However, no measurable differences in the densities of the slowly activating, noninactivating current, I_{ss}, and hyperpolarization-activated, inwardly rectifying K^+ current, I_{K1}, were observed in WT and N-cad CKO myocytes (Fig. 3, *B* and *D*).

$I_{K,slow}$ Is Attenuated Selectively in N-cad CKO Ventricular Myocytes—The decay phases of the Kv currents in adult WT and N-cad CKO mouse ventricular myocytes are well described by the sum of two exponentials, reflecting the fast components of inactivation ($I_{to,f}$), the slow components of inactivation ($I_{K,slow}$), and a noninactivating current (I_{ss}) (supplemental Fig. S1) (24, 26). Decay time constants (τ_{decay}) at +40 mV for the fast and the slow components of inactivation in WT cells ($n = 24$) were 124 ± 9 and 1311 ± 52 ms (supplemental Table S2). In the N-cad CKO group, the mean decay time constants were similar to WT (supplemental Table 2). Analysis of the decay phases of

the outward currents also revealed that the density of the slow component of current decay in N-cad CKO ventricular cells was lower than in WT cells; mean ± S.E. $I_{K,slow}$ densities (at +40 mV) were reduced by ~47% in ventricular cells isolated from N-cad CKO compared with WT littermates, respectively (Fig. 3*E*). The percentage of the slow component of current decay of the total current decreased from 55 ± 1% in WT to 43 ± 1% in N-cad CKO ventricular cells, which further proved decreased $I_{K,slow}$ densities in N-cad CKO group. Mean whole cell membrane capacitance (C_m) in WT (180 ± 8 pF, $n = 60$) and N-cad CKO (159 ± 9 pF, $n = 37$) ventricular myocytes were not significantly different. Therefore, the reduced $I_{K,slow}$ current density does not result from cellular enlargement. In contrast, no measurable differences in the densities of the fast transient Kv current, $I_{to,f}$, were found at + 40 mV ($p = 0.19$; Fig. 3*E*). No significant differences in the densities of the steady-state outward K^+ currents, I_{ss}, determined as the currents remaining at the end of 4.5-s voltage steps, were observed.

There are several factors contributing macroscopic ion currents amplitude: numbers of the channel, channel open probabilities, activation or inactivation kinetics, activation or inactivation voltage dependence, and single channel conductance. There were no significant differences in activation or inactivation kinetics, or voltage dependence, observed between WT and N-cad CKO animals (data not shown). Although the above results strongly suggest that $I_{K,slow}$ is selectively attenuated in ventricular myocytes from N-cad CKO animals, these data did not themselves rule out a contribution of single channel conductance or any alterations either from other channels or transporters (*e.g.* Na^+ channel).

Kv1.5 Channel and Kcne2 Were Reduced in N-cad CKO Ventricular Myocytes—To test directly the idea that ion channel remodeling was caused by altered expression and distribution of Kv channels and auxiliary subunits, confocal Z-scan images were quantified as described previously (18). Although Kv1.5 staining in WT adult ventricular myocytes could be seen extensively throughout the cell surface and at Z-lines, it was also localized prominently in the ICD (Fig. 4*A*), as reported previously (27, 28). In contrast, in N-cad CKO ventricular myocytes Kv1.5 appeared absent from the ICD (Fig. 4*B*). In addition, overall expression of Kv1.5 was decreased in N-cadherin-deficient cells relative to WT (Fig. 4, *A* and *B*). Mean fluorescence signal intensity of Kv1.5 at or near the cell surface, quantitated using the histogram function in National Institutes of Health ImageJ software, was ~58% lower in N-cad CKO (96.8 ± 11.9, $n = 15$) compared with WT (232.3 ± 12.2, $n = 15$) ventricular myocytes (Fig. 4*I*). Moreover, the Kv1.5 ancillary subunit, Kcne2, was also reduced ~66% in N-cad CKO (72.3 ± 12.8, $n = 18$) compared with WT (216.5 ± 14.5, $n = 16$) ventricular myocytes (Fig. 4, *C* and *D*). Thus, immunofluorescence experiments yielded data consistent with the whole cell patch clamping results. In contrast, Kir2.1 channel, which encodes I_{K1}, was not affected in N-cad CKO myocytes (Fig. 4, *G* and *H*). The immunostaining pattern for other murine Kv channels such as Kv1.4 (Fig. 4, *E* and *F*), Kv2.1, Kv4.2, and Kv4.3, as well as auxiliary subunit KChIP2 were affected to different degrees in N-cad CKO myocytes (supplemental Fig. S2).

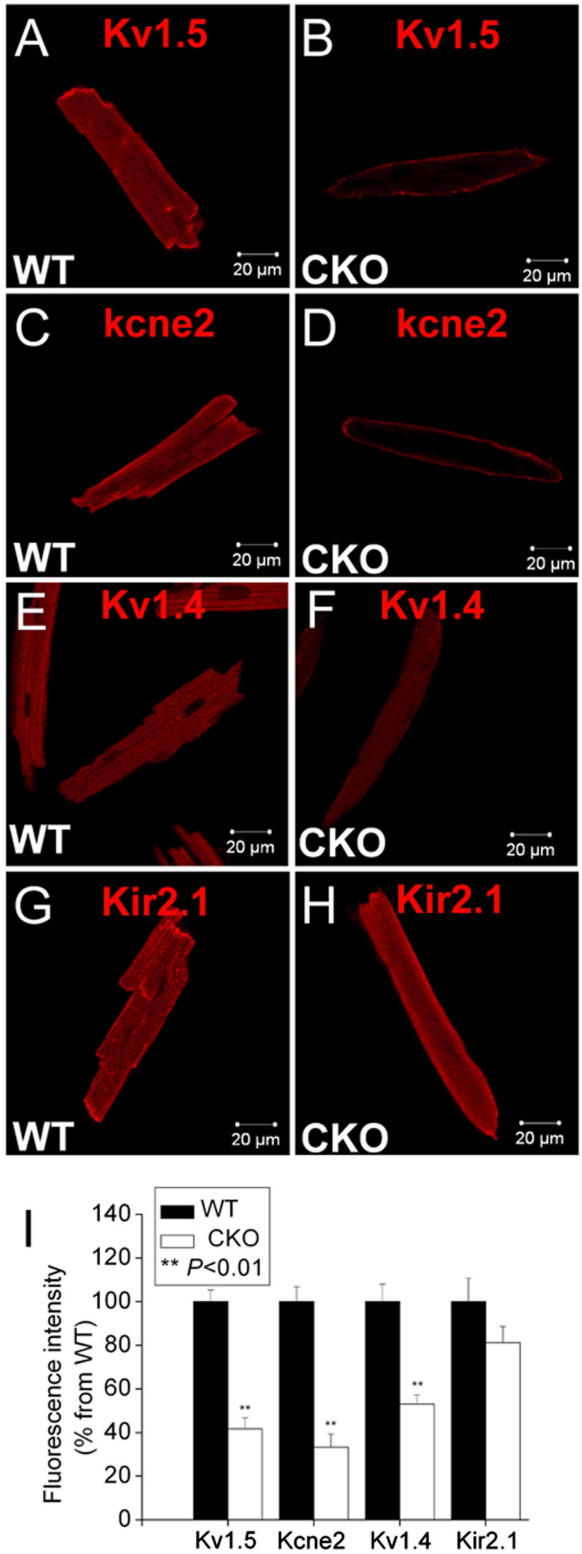

FIGURE 4. **Differential expression of Kv channels in N-cad CKO myocytes.** *A–H*, immunostaining of Kv1.5 (*A* and *B*), kcne2 (*C* and *D*), Kv1.4 (*E* and *F*), and Kir2.1 (*G* and *H*) in WT and N-cad CKO. *I*, relative cell surface fluorescence intensity was quantified from eight optical slices through the cardiomyocyte ($n = 10–12$). **, $p < 0.01$, one-way analysis of variance.

To determine whether Kv1.5 and KCNE2 expression was affected at the mRNA level, quantitative RT-PCR was performed on N-cad CKO hearts. The mRNA levels of the different

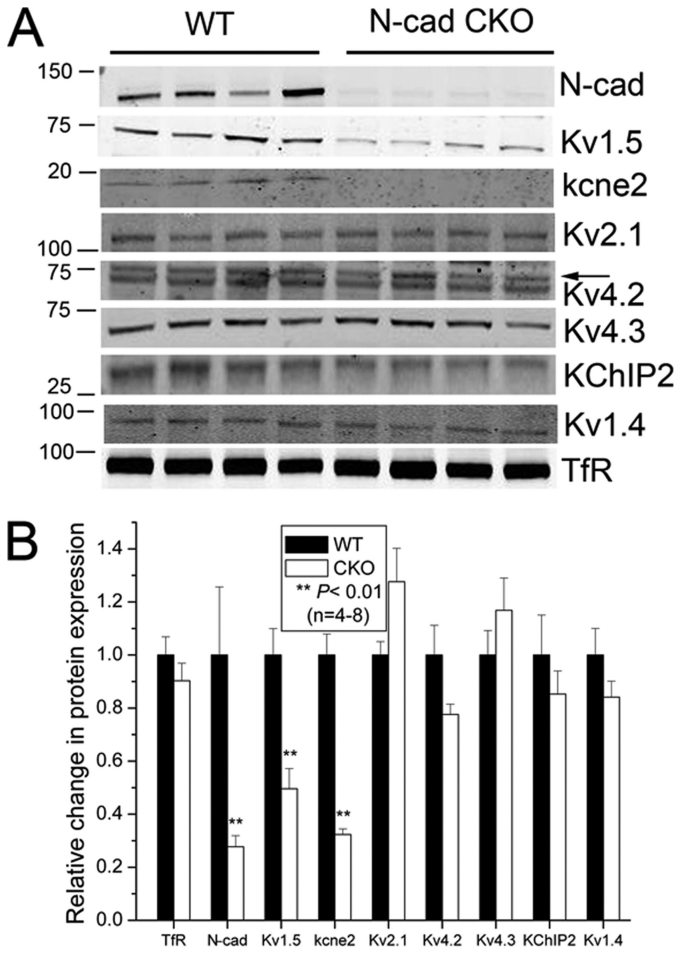

FIGURE 5. **Kv1.5 and kcne2 expression were reduced in N-cad CKO ventricles.** *A*, quantitative Western blot analysis was performed on fractionated ventricular membrane from WT and N-cad CKO hearts. *B*, quantification of the Western blot data. Transferrin receptor signal was used to normalize for loading differences between lanes.

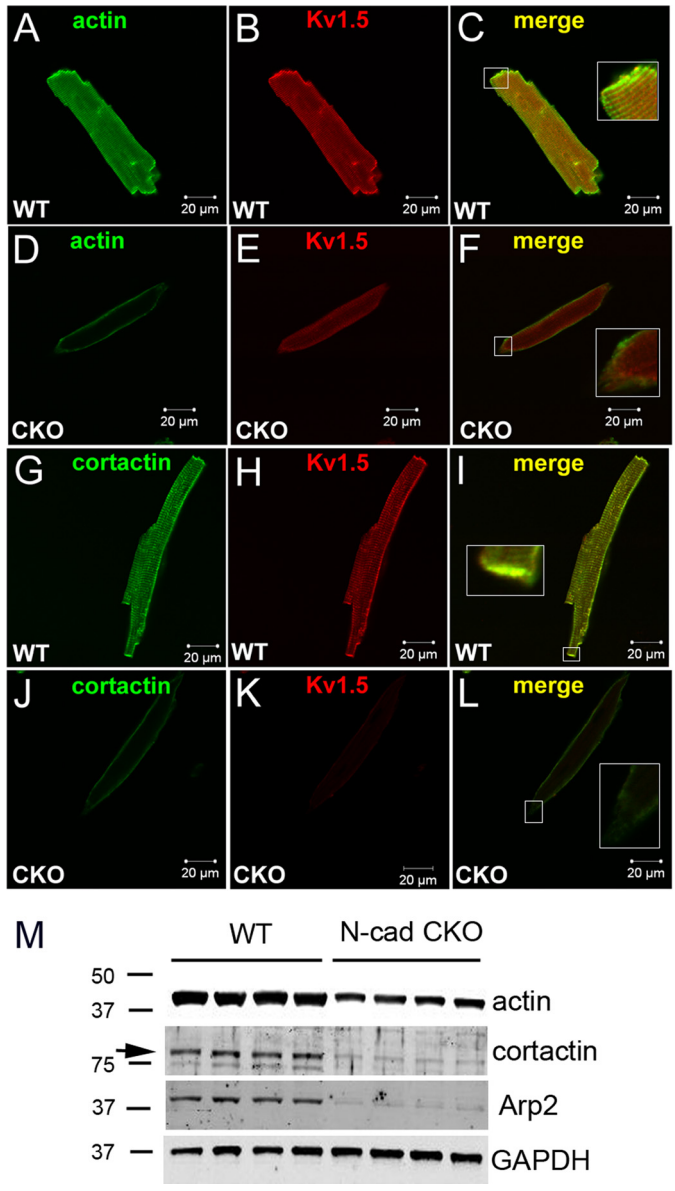

FIGURE 6. **Disruption of cortactin-actin cytoskeleton organization in N-cad CKO ventricular myocytes.** Cardiomyocytes from WT and N-cad CKO mice were co-stained for actin (*A* and *D*) and Kv1.5 (*B* and *E*) or cortactin (*G* and *J*) and Kv1.5 (*H* and *K*). *C*, *F*, *I*, and *L*, *insets* show higher magnification of intercalated disc staining. *M*, Western blot analysis of actin, cortactin, and Arp2 in cortical cytoskeleton enriched fractions from WT and N-cad CKO ventricles. The *arrow* denotes the protein band corresponding to cortactin targeted by the antibody.

channel components did not change, indicating that post-transcriptional regulation was responsible for their decreased expression after N-cadherin depletion (supplemental Fig. S3).

Biochemical experiments were then performed to examine sarcolemma expression of Kv channels and auxiliary subunits in the absence of N-cadherin. Membrane fraction preparations were confirmed by the presence of TfR protein, which is absent in cytosol fraction (data not shown). Because no change in TfR protein expression was observed in the N-cad CKO compared with WT (Fig. 5), TfR protein was used as protein loading control. Western blot analysis demonstrated markedly reduced Kv1.5 membrane expression in N-cad CKO hearts (−50% *versus* controls; $p < 0.01$; $n = 8$) (Fig. 5). The reduction in Kv1.5 protein expression is consistent with the observed reduction in $I_{K,slow}$ in the N-cad CKO myocytes. In parallel with the decrease in Kv1.5, the auxillary subunit, Kcne2, was also reduced in N-cad CKO (−67% *versus* controls; $p < 0.01$; $n = 8$), whereas there were no detectable differences in Kv2.1, Kv4.2, Kv4.3, KChIP2, and Kv1.4 (Fig. 5).

Remodeling of Kv Channels Is Associated with Disruption of Actin Cytoskeleton in N-cad CKO Myocytes—Recent evidence suggests that Kv channel α and accessory (β) subunit assemblies associate with the actin cytoskeleton (29, 30). These interactions likely are important in determining channel stability, trafficking, localization, and biophysical properties. N-cadherin is localized predominantly to the ICD; however, Kv channels were reduced not only at the ICD but throughout the sarcolemma, suggesting a global cellular change occurred in the N-cad CKO cardiomyocytes. We speculated that disruption of the actin cytoskeleton might account for Kv channel remodeling in N-cad CKO myocytes. To address this possibility, Kv1.5 and actin organization were examined in isolated cardiomyocytes using an antibody directed against all actin subunits. Disruption of actin cytoskeleton organization correlated with decreased Kv1.5 expression in N-cad CKO ventricular myocytes, as evidenced by a loss of striation pattern and a general

dispersal of actin staining (Fig. 6, *A* and *D*). Moreover, we observed a positive correlation between the relative intensity of actin and Kv1.5 immunoreactivity at the cell surface in the N-cadherin-deficient cardiomyocytes (supplemental Fig. S4). Mean fluorescence signal intensity of actin at or near the cell surface, quantitated using National Institutes of Health ImageJ software, was ~68% lower in N-cad CKO (63 ± 13, $n = 24$) compared with WT (198 ± 25, $n = 17$) ventricular myocytes. A similar result was obtained with a different antibody directed against cardiac-specific actin (data not shown).

Cadherin and cortactin, an actin filament-binding protein, cooperate to mediate actin reorganization and adhesion strength (31). Initially, we examined whether cortactin was affected in the N-cad CKO myocytes. Remarkably, Kv1.5 and cortactin were co-localized in WT cardiomyocytes including the ICD (Fig. 6, *G–I*). In contrast, N-cad CKO ventricular myocytes displayed weak or absent Kv1.5/cortactin co-localization (Fig. 6, *J–L*). *N-cadherin* gene deletion dramatically reduced fluorescence signal intensity of cortactin (−82%, $p < 0.01$) at or near the cell surface in N-cad CKO (44 ± 5, $n = 11$) (Fig. 6*G*) compared with WT (243 ± 28, $n = 11$) (Fig. 6*J*). Western analysis of the cortical cytoskeleton enriched fraction demonstrated reduction of both actin and cortactin (Fig. 6*M*) consistent with the immunofluorescence data. In addition, the cortactin-binding protein, Arp2 (32), was also reduced in the N-cad CKO hearts (Fig. 6*M*). In contrast, sarcomeric α-actinin expression and distribution were not affected by the loss of N-cadherin (supplemental Fig. S5).

Cortactin Associates with Kv1.5 Channel—It was previously reported that cortactin associates with Kv1.2 channel in the brain (19); therefore we performed immunoprecipitation experiments to determine whether cortactin associated with Kv1.5 channel. For these studies, a cortical cytoskeleton enriched fraction was prepared on both transfected HEK-293 cells expressing Kv1.5-GFP fusion protein and adult mouse ventricles as reported previously (19). A polyclonal anti-cortactin antibody was used to immunoprecipitate Kv1.5 and associated proteins in extracts prepared from HEK-293 cells transiently transfected with Kv1.5-GFP. The association of cortactin with Kv1.5-GFP fusion protein was demonstrated by immunoblotting for both Kv1.5 and GFP (Fig. 7*A*, *upper panel*). In addition, cortactin was detected in the anti-GFP antibody immunoprecipitate (Fig. 7*A*, *lower panel*). To examine the interaction between cortactin and Kv1.5 in the native tissue, extracts of adult mouse ventricles were immunoprecipitated with the anti-cortactin antibody and immunoblotted with anti-Kv1.5 antibody. As observed in the heterologous system, cortactin associates with Kv1.5 in the heart (Fig. 7*B*, *upper panel*). N-cadherin was not detected in the cortactin immunoprecipitate. Furthermore, immunoprecipitation with anti-N-cadherin antibody did not immunoprecipitate cortactin or Kv1.5 in the heart; however, the cadherin-binding protein β-catenin was present (Fig. 7*B*, *lower panel*).

Cortactin Is Required for N-cadherin-mediated Kv1.5 Channel Activity—Because both cortactin and Kv1.5 channel were decreased in N-cad CKO cardiomyocytes, we hypothesized that depleting intracellular cortactin would cause suppression of Kv1.5 ionic current in the presence of N-cadherin. First, we

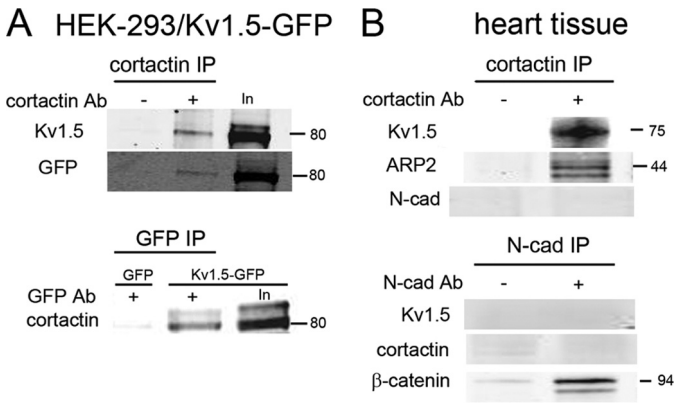

FIGURE 7. **Cortactin associates with Kv1.5 channel.** *A*, *upper panel*, extracts of HEK-293 cells transfected with Kv1.5-GFP were immunoprecipitated (*IP*) using a polyclonal anti-cortactin antibody and immunoblotted with anti-Kv1.5 antibody first and then stripped and reprobed with anti-GFP antibody. Total input (*In*) HEK-293/Kv1.5-GFP cell extract was also probed with anti-Kv1.5 and anti-GFP antibodies. Immunoprecipitation minus cortactin antibody was used as a negative control. *Lower panel*, to control for nonspecific binding of cortactin to GFP, HEK-293 cells were transfected with GFP or Kv1.5-GFP followed by immunoprecipitation with anti-GFP antibody and immunoblotted for cortactin. Total input (*In*) HEK-293/Kv1.5-GFP cell extract was also probed with the anti-cortactin antibody. Note that GFP alone does not interact with cortactin. *B*, *upper panel*, extracts of adult mouse ventricles were immunoprecipitated with anti-cortactin antibody and immunoblotted with anti-Kv1.5, anti-Arp2, and anti-N-cadherin antibodies. *Lower panel*, extracts of adult mouse ventricles were immunoprecipitated with anti-N-cadherin antibody and immunoblotted with anti-Kv1.5, anti-cortactin, and anti-β-catenin antibodies. As a direct binding partner of N-cadherin, β-catenin was used as a positive control.

determined that regulation of N-cadherin was specific to Kv1.5 channel rather than other murine Kv channels. *Xenopus* oocytes were injected simultaneously with equal amounts of cRNA encoding N-cadherin along with cRNA encoding Kv1.5, Kv2.1, or Kv4.2 wild type channels. Voltage clamp measurements revealed a significant enhancement of Kv1.5 ionic current in oocytes co-injected with N-cadherin relative to control (Fig. 8*A*). However, co-expression of N-cadherin with Kv2.1 or Kv4.2 did not enhance channel activity (Fig. 8, *B* and *C*). Then *Xenopus* oocytes were injected simultaneously with antisense DNA oligonucleotides directed against *Xenopus* cortactin and with cRNA encoding N-cadherin and Kv1.5 channel. Voltage clamp measurements revealed a significant suppression of Kv1.5 ionic current in oocytes injected with antisense cortactin oligonucleotides relative to control (Fig. 9), indicating a key role for cortactin in mediating the N-cadherin effect on Kv1.5 channel function.

DISCUSSION

This study demonstrates for the first time that cardiac-specific deletion of N-cadherin results in ventricular Kv channel remodeling, which together with gap junction remodeling likely contributes to the arrhythmogenic phenotype in the N-cad CKO mice. Reduction in the densities of specific K^+ currents in the N-cad CKO myocytes was associated with alterations in the expression of the subunits underlying these currents. In the biochemical analyses completed here, down-regulation of Kv1.5 channels surface expression was observed, consistent with the markedly reduced $I_{K,slow}$ amplitude in N-cad CKO myocytes. Importantly, no detectable change in cell surface protein expression of Kv2.1 (another subunit

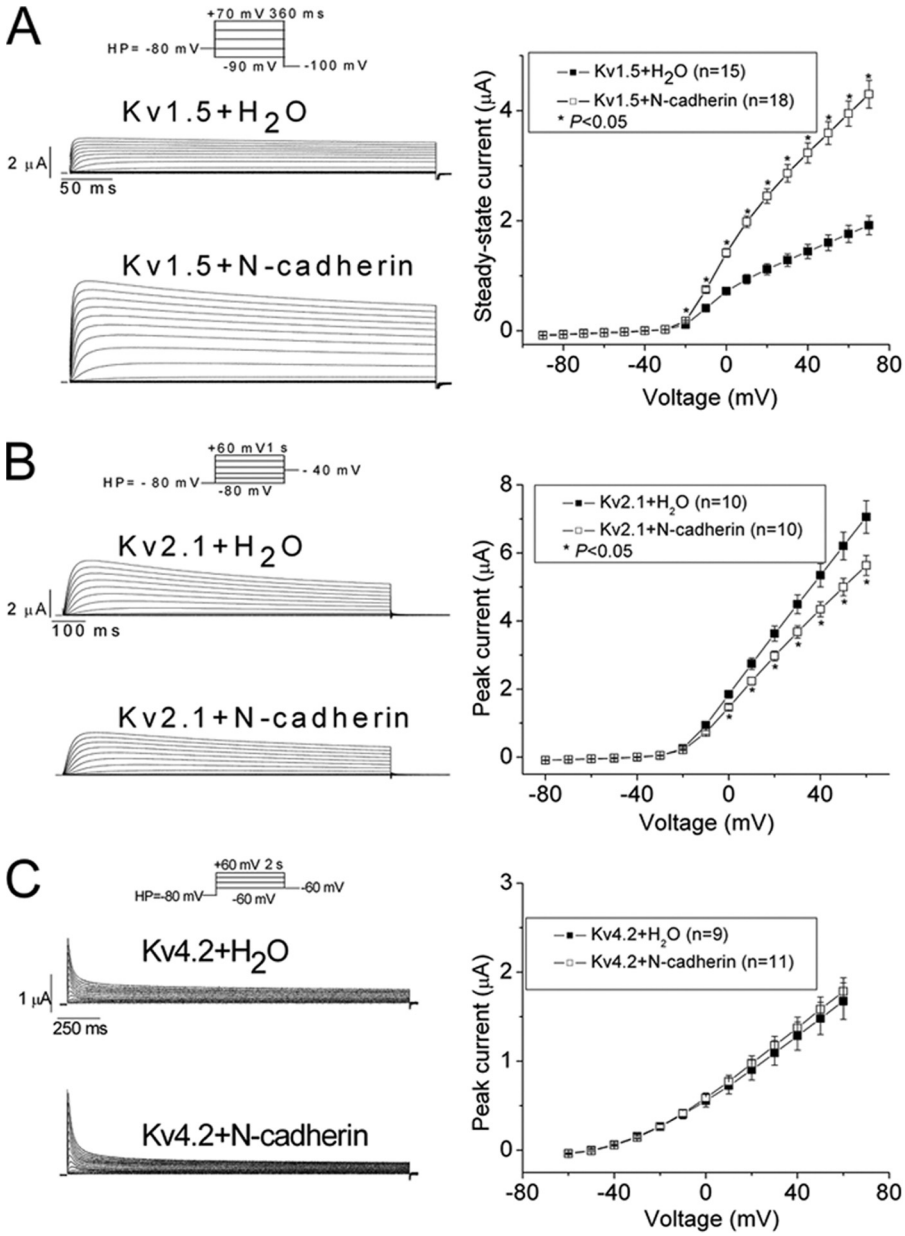

FIGURE 8. **N-cadherin specifically enhanced Kv1.5 currents.** cRNA encoding Kv1.5 and Kv1.5+ N-cad (*A*), Kv2.1 and Kv2.1+N-cad (*B*), and Kv4.2 and Kv4.2+N-cad (*C*) was injected into *Xenopus* oocytes. The details of the voltage clamp protocols are described in the legends (not to scale). In general, to record the current-voltage (*I-V*) relationship, the oocytes were voltage-clamped at a negative holding potential (−80 mV). Test potentials were applied to a variable potential with a fixed incremental increase between successive pulses at variable durations.

underlying $I_{K,slow}$) was found. This negative finding indicates that the reduction of Kv1.5 channel surface expression is likely responsible for the change in $I_{K,slow}$. Although the specificity of the anti-Kv1.5 antibody used to detect endogenous Kv1.5 in cardiomyocytes is a concern in the field (33, 34), the combined use of whole cell recording, immunostaining, and immunoblotting provides a more solid and specific interpretation of Kv1.5 channel remodeling in the N-cad CKO model. In contrast to $I_{K,slow}$, I_{ss} and I_{K1} densities were not significantly different. Although trending toward a statistical difference ($p = 0.19$), there is no significant change in $I_{to,f}$ in N-cad CKO myocytes. There was no detectable change in Kv4.2, Kv4.3, and KChIP2 expression by Western blot of membrane fractions; however, immunofluorescence analysis suggested these channels were affected in the N-cad CKO, albeit, to a lesser degree than Kv1.5. One explanation for this apparent discrepancy between the Western and immunofluorescence results is based on our observation that although all cardiomyocytes lost N-cadherin, the actin remodeling appeared heterogeneous among the mutant cardiomyocytes (supplemental Fig. S4). Interestingly, we did observe that the actin change was more extensive in N-cad CKO myocytes isolated at 5 weeks compared with 4 weeks post Tam, suggesting the cytoskeletal change was progressive. Because of the short lifespan of the N-cad CKO mice (animals begin to exhibit sudden cardiac death 5 weeks post Tam), it was not possible to follow the actin remodeling any further. Importantly, only myocytes with altered actin cytoskeleton had the corresponding change in Kv1.5 channel distribu-

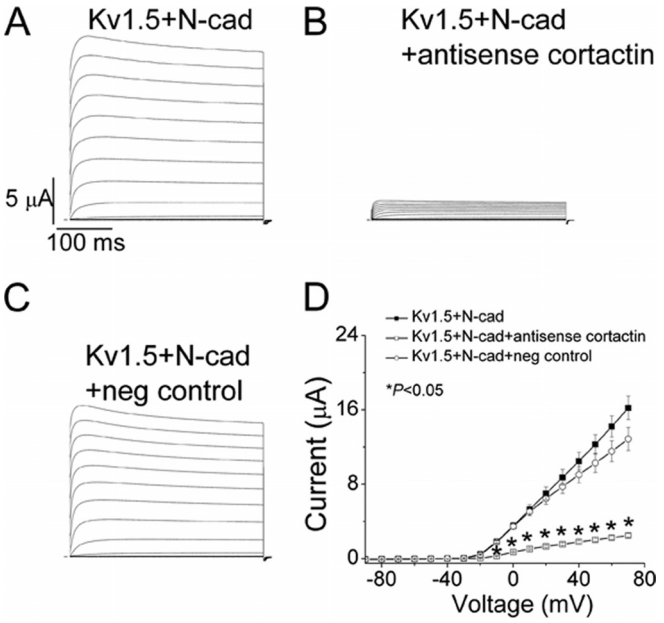

FIGURE 9. **Knockdown of cortactin ablated the N-cadherin regulation of Kv1.5 channel activity.** *A*, ionic current generated by injecting cRNA encoding Kv1.5 and N-cadherin in *Xenopus* oocytes. *B*, co-injection of *Xenopus* cortactin-specific antisense DNA oligonucleotides with cRNA encoding Kv1.5 and N-cadherin. *C*, co-injection with scrambled control oligonucleotides showed no effect on current enhancement by N-cadherin. *D*, average current-voltage relationships in different groups. ■, Kv1.5 + N-cadherin, $n = 16$; □, Kv1.5 + N-cadherin +cortactin-specific antisense DNA oligonucleotides, $n = 30$; ○, Kv1.5 + N-cadherin + negative control, $n = 18$.

tion, suggesting that the cytoskeletal change preceded Kv channel remodeling. In contrast, ventricular membrane fractions represent all the cardiomyocytes regardless of the extent of the actin remodeling; thus only the most affected channels (*i.e.* Kv1.5) show a change by Western blot. The same is true for the selection of cardiomyocytes for patch clamp recording. Although the N-cad CKO myocytes have an abnormal cell shape (*i.e.* more spindle-like), it is not possible to determine which myocytes exhibit the actin remodeling based only on morphological criteria. Therefore, the patch clamp recordings likely include myocytes with modest cytoskeletal change, thus possibly underestimating a change in $I_{to,f}$.

Kv1.5 Channel and Arrhythmia—Previous studies demonstrated the contribution of Kv1.5 channel to the repolarization of the cardiac action potential (35, 36). In atrial myocytes from patients with valvular disease and persistent atria fibrillation, it was observed that the sustained K^+ current was reduced by ~50%, and there was a parallel reduction in the expression of Kv1.5 protein (37). Interestingly, N-cad CKO mice also show atria fibrillation (8), which could be related to reduced Kv1.5 expression in atria, although we have limited this study to ventricular myocytes. Loss-of-function Kv1.5 mutations (Kv1.5W461F) were shown to contribute to increased ventricular action potential durations (APD_{75} and APD_{95}) and marked QT prolongation (35). Furthermore, mice with a long QT phenotype showed improved action potential duration upon adenoviral expression of Kv1.5 (38). The loss of Kv1.5 alone is not arrhythmogenic *per se* (36); however, recent studies have highlighted the importance of repolarization abnormalities, including nonuniform prolongation of action potential durations across the ventricular wall. Such repolarization changes may lead to the development of reentrant arrhythmias (39). When considering the prerequisites for reentry, however, two conditions must be met: (*a*) the excitation wavefront must undergo unidirectional conduction block and (*b*) the path of the reentrant circuit must be sufficiently long or conduction of the wavefront sufficiently slow, such that each site along the circuit has ample opportunity to regain excitability before the return of the circulating wave to avoid collision and extinction. Our previous optical mapping reveals reduced conduction velocity in the N-cadherin CKO hearts, consistent with down-regulation of Cx43 (8). We hypothesize that slowed conduction velocity in combination with repolarization abnormalities promotes the development of potentially lethal reentrant ventricular arrhythmias in the N-cad CKO model.

Ion Channels and ICD—Recent evidence suggests that the structural integrity of ICD is critical for maintaining both mechanical and electrical coupling in the myocardium (7, 8). Several channels and transporters have been found to be largely localized to the intercalated disc, including Kv1.5 (27). The $Na_v1.5$ sodium channel resident at the intercalated disc has been suggested to play a role in initiation and conduction of the action potential (40, 41). Knockdown of plakophilin-2, an essential component of the desmosome, leads to decreased sodium current and slower conduction velocity in cultured cardiac myocytes (42). However, the localization of Kv channels in cardiomyocytes as well as the relationship with ICD proteins remains undefined. It was reported that the results of Kv1.5 localization studies are very much dependent upon the anti-Kv1.5 antibody used and species (43). The distribution of Kv1.5 in our study is consistent across studies that Kv1.5 staining in mouse appears to be generally at the cell surface and at Z-lines, at least in WT ventricular myocytes (44). N-cadherin-deficient cardiomyocytes lost the characteristic interdigitating or step-like structures at the termini representing the ICD, together with Kv1.5 channel, providing a functional link between ICD structure and Kv channel localization at the sarcolemma. A previous study showed that co-expression of N-cadherin and Kv1.5 in *Xenopus* oocytes increases the induced outward current by ~2.5-fold (45). In this gain-of-function experiment, there was no apparent change in Kv1.5 channel cell surface expression. Instead, N-cadherin enhances the Kv1.5 current by promoting recovery from slow inactivation. This result appears to conflict with our loss-of-function studies, where Kv1.5 expression is reduced at the sarcolemma in the N-cadherin-null cardiomyocytes. Presently, we do not know why the native and heterologous systems produce apparently different mechanistic results.

In support of our findings, it was shown that an ancillary potassium channel subunit Kcne2 enhanced Kv1.5 channel trafficking to ICD (46). Targeted deletion of Kcne2 impaired ventricular repolarization via selective disruption of $I_{K,slow1}$, generated by Kv1.5, and $I_{to,f}$, generated by Kv4 α subunits (46). Our results are consistent with these studies because we also observed down-regulation of surface Kcne2 and selective disruption of $I_{K,slow}$ in N-cad CKO cardiomyocytes.

Potential Roles of Cortactin-actin Cytoskeleton in Regulating Kv1.5 Channel Function—Mounting evidence indicates that the cytoskeleton is central to determining the localization and functional activity of many ion channels (29, 47, 48). N-cadherin regulates actin cytoskeletal dynamics via its interaction with catenins and other actin-binding proteins (5, 6). We show that a proportion of N-cadherin-deficient cardiomyocytes exhibit a disorganized actin cytoskeleton including a decrease in cortical actin that correlates with Kv channel remodeling. The actin cytoskeleton has been implicated in Kv1.5 channel endocytosis (49), but its necessity and roles in Kv1.5 channel surface distribution and expression remain ambiguous. Importantly, the cortical actin scaffold protein, cortactin, associates with Kv1.2 and plays an essential role in regulating its cell surface expression (19, 20). In addition, cortactin can also modulate expression of the voltage- and calcium-activated potassium (BK) channels (50). Our co-immunoprecipitation experiments using both heterologous and native heart tissue identified an association between cortactin and Kv1.5. Because cortactin affects Kv1.2 endocytosis in mammalian cells (20), future studies will focus on the role of cortactin in Kv1.5 channel trafficking. Functionally, knockdown of cortactin ablated the regulation of Kv1.5 channel activity by N-cadherin in the oocyte expression system, strongly supporting the idea of an N-cadherin-cortical actin-cortactin-Kv1.5 axis. In nonmyocytes, cortactin has been shown to interact with the cadherin-catenin complex (51, 52); however, we did not detect N-cadherin-cortactin association by co-immunoprecipitation in heart tissue. This result suggests that N-cadherin-cortactin association is cell type-dependent. Because of the requirement of cortactin in embryonic development (53), a conditional knock-out model will be required in the future to study its function in the heart.

In conclusion, these data indicate that a loss of N-cadherin alters the actin cytoskeleton, leading to a decrease in the cortical actin-binding protein, cortactin, which associates with Kv1.5 channel and regulates its function in the heart. These studies demonstrate for the first time that a loss of N-cadherin contributes to arrhythmogenesis not only through conduction slowing but also through remodeling of the major outward potassium currents.

Acknowledgments—We are grateful to Drs. Joseph Cheung, Gregory Morley, and Michael C. Sanguinetti for comments on the manuscript; Dr. Joseph Cheung's lab for pilot action potential recordings; Dr. Guiscard Seebohm for Kv channel cDNA clones; Dr. Nancy Philp for fruitful discussion; Dr. Jeanne Nerbonne for suggestions on data analysis; Dr. Anthony Morielli for advice on cortactin-enriched fraction preparation; Dr. Kurt Chuprun for help with membrane fraction preparation; Annika Barber and Brian Urbani for oocyte isolation; Dave Swope for advice about RT-PCR; and Craig Riley, David Kurz, Leeanne Griffith, and Andrew Ho for technical assistance. We thank Dr. Maria Yolanda Covarrubias (Bioimaging Facility of the Kimmel Cancer Center) for confocal imaging.

REFERENCES

1. Ackerman, M. J., and Mohler, P. J. (2010) *Circ. Res.* **107,** 457–465
2. Steele, D. F., Eldstrom, J., and Fedida, D. (2007) *J. Physiol.* **582,** 17–26
3. Delmar, M., and McKenna, W. J. (2010) *Circ. Res.* **107,** 700–714
4. Saffitz, J. E. (2006) *J. Cardiovasc. Electrophysiol.* **17,** 225–229
5. Meng, W., and Takeichi, M. (2009) *Cold Spring Harb. Perspect. Biol.* 1:a002899
6. Nelson, W. J. (2008) *Biochem. Soc. Trans.* **36,** 149–155
7. Kostetskii, I., Li, J., Xiong, Y., Zhou, R., Ferrari, V. A., Patel, V. V., Molkentin, J. D., and Radice, G. L. (2005) *Circ. Res.* **96,** 346–354
8. Li, J., Patel, V. V., Kostetskii, I., Xiong, Y., Chu, A. F., Jacobson, J. T., Yu, C., Morley, G. E., Molkentin, J. D., and Radice, G. L. (2005) *Circ. Res.* **97,** 474–481
9. Tomaselli, G. F., and Zipes, D. P. (2004) *Circ. Res.* **95,** 754–763
10. Jeron, A., Mitchell, G. F., Zhou, J., Murata, M., London, B., Buckett, P., Wiviott, S. D., and Koren, G. (2000) *Am. J. Physiol. Heart Circ. Physiol.* **278,** H1891–H1898
11. Gutstein, D. E., Morley, G. E., Vaidya, D., Liu, F., Chen, F. L., Stuhlmann, H., and Fishman, G. I. (2001) *Circulation* **104,** 1194–1199
12. Zemljic-Harpf, A. E., Miller, J. C., Henderson, S. A., Wright, A. T., Manso, A. M., Elsherif, L., Dalton, N. D., Thor, A. K., Perkins, G. A., McCulloch, A. D., and Ross, R. S. (2007) *Mol. Cell. Biol.* **27,** 7522–7537
13. Zhou, Y. Y., Wang, S. Q., Zhu, W. Z., Chruscinski, A., Kobilka, B. K., Ziman, B., Wang, S., Lakatta, E. G., Cheng, H., and Xiao, R. P. (2000) *Am. J. Physiol. Heart Circ. Physiol.* **279,** H429–H436
14. Bean, B. P. (2007) *Nat. Rev. Neurosci.* **8,** 451–465
15. Livak, K. J., and Schmittgen, T. D. (2001) *Methods* **25,** 402–408
16. London, B., Jeron, A., Zhou, J., Buckett, P., Han, X., Mitchell, G. F., and Koren, G. (1998) *Proc. Natl. Acad. Sci. U.S.A.* **95,** 2926–2931
17. Li, J., Levin, M. D., Xiong, Y., Petrenko, N., Patel, V. V., and Radice, G. L. (2008) *J. Mol. Cell Cardiol.* **44,** 597–606
18. Choi, W. S., Khurana, A., Mathur, R., Viswanathan, V., Steele, D. F., and Fedida, D. (2005) *Circ. Res.* **97,** 363–371
19. Hattan, D., Nesti, E., Cachero, T. G., and Morielli, A. D. (2002) *J. Biol. Chem.* **277,** 38596–38606
20. Williams, M. R., Markey, J. C., Doczi, M. A., and Morielli, A. D. (2007) *Proc. Natl. Acad. Sci. U.S.A.* **104,** 17412–17417
21. Shahidullah, M., Harris, T., Germann, M. W., and Covarrubias, M. (2003) *Biochemistry* **42,** 11243–11252
22. Jerng, H. H., Shahidullah, M., and Covarrubias, M. (1999) *J. Gen. Physiol.* **113,** 641–660
23. Nerbonne, J. M., and Guo, W. (2002) *J Cardiovasc. Electrophysiol.* **13,** 406–409
24. Xu, H., Guo, W., and Nerbonne, J. M. (1999) *J. Gen. Physiol.* **113,** 661–678
25. Zaritsky, J. J., Redell, J. B., Tempel, B. L., and Schwarz, T. L. (2001) *J. Physiol.* **533,** 697–710
26. Marionneau, C., Aimond, F., Brunet, S., Niwa, N., Finck, B., Kelly, D. P., and Nerbonne, J. M. (2008) *J. Mol. Cell Cardiol.* **44,** 1002–1015
27. Mays, D. J., Foose, J. M., Philipson, L. H., and Tamkun, M. M. (1995) *J. Clin. Invest.* **96,** 282–292
28. Murata, M., Buckett, P. D., Zhou, J., Brunner, M., Folco, E., and Koren, G. (2001) *Am. J. Physiol. Heart Circ Physiol.* **281,** H2575–H2584
29. Shimoni, Y., Ewart, H. S., and Severson, D. (1999) *J Physiol* **514,** 735–745
30. Yang, X., Salas, P. J., Pham, T. V., Wasserlauf, B. J., Smets, M. J., Myerburg, R. J., Gelband, H., Hoffman, B. F., and Bassett, A. L. (2002) *J. Physiol.* **541,** 411–421
31. El Sayegh, T. Y., Arora, P. D., Fan, L., Laschinger, C. A., Greer, P. A., McCulloch, C. A., and Kapus, A. (2005) *Mol. Biol. Cell* **16,** 5514–5527
32. Weed, S. A., Karginov, A. V., Schafer, D. A., Weaver, A. M., Kinley, A. W., Cooper, J. A., and Parsons, J. T. (2000) *J. Cell Biol.* **151,** 29–40
33. Eldstrom, J., Van Wagoner, D. R., Moore, E. D., and Fedida, D. (2006) *FEBS Lett.* **580,** 6039–6046
34. Marionneau, C., Brunet, S., Flagg, T. P., Pilgram, T. K., Demolombe, S., and Nerbonne, J. M. (2008) *Circ. Res.* **102,** 1406–1415
35. Li, H., Guo, W., Yamada, K. A., and Nerbonne, J. M. (2004) *Am. J. Physiol. Heart Circ. Physiol.* **286,** H319–H328
36. London, B., Guo, W., Pan, Xh., Lee, J. S., Shusterman, V., Rocco, C. J., Logothetis, D. A., Nerbonne, J. M., and Hill, J. A. (2001) *Circ. Res.* **88,** 940–946
37. Van Wagoner, D. R., Pond, A. L., McCarthy, P. M., Trimmer, J. S., and Nerbonne, J. M. (1997) *Circ. Res.* **80,** 772–781
38. Brunner, M., Kodirov, S. A., Mitchell, G. F., Buckett, P. D., Shibata, K.,

Folco, E. J., Baker, L., Salama, G., Chan, D. P., Zhou, J., and Koren, G. (2003) *Am. J. Physiol. Heart Circ Physiol* **285,** H194–H203
39. Akar, F. G., and Rosenbaum, D. S. (2003) *Circ. Res.* **93,** 638–645
40. Kucera, J. P., Rohr, S., and Rudy, Y. (2002) *Circ. Res.* **91,** 1176–1182
41. Maier, S. K., Westenbroek, R. E., Schenkman, K. A., Feigl, E. O., Scheuer, T., and Catterall, W. A. (2002) *Proc. Natl. Acad. Sci. U.S.A.* **99,** 4073–4078
42. Sato, P. Y., Musa, H., Coombs, W., Guerrero-Serna, G., Patiño, G. A., Taffet, S. M., Isom, L. L., and Delmar, M. (2009) *Circ. Res.* **105,** 523–526
43. Fedida, D., Eldstrom, J., Hesketh, J. C., Lamorgese, M., Castel, L., Steele, D. F., and Van Wagoner, D. R. (2003) *Circ. Res.* **93,** 744–751
44. Mathur, R., Choi, W. S., Eldstrom, J., Wang, Z., Kim, J., Steele, D. F., and Fedida, D. (2006) *Biochem. Biophys. Res. Commun.* **342,** 1–8
45. Koutsouki, E., Lam, R. S., Seebohm, G., Ureche, O. N., Ureche, L., Baltaev, R., and Lang, F. (2007) *Biochem. Biophys. Res. Commun.* **363,** 18–23
46. Roepke, T. K., Kontogeorgis, A., Ovanez, C., Xu, X., Young, J. B., Purtell, K., Goldstein, P. A., Christini, D. J., Peters, N. S., Akar, F. G., Gutstein, D. E., Lerner, D. J., and Abbott, G. W. (2008) *FASEB J.* **22,** 3648–3660
47. Cunha, S. R., and Mohler, P. J. (2008) *Circ. Res.* **103,** 779–781
48. Undrovinas, A. I., Shander, G. S., and Makielski, J. C. (1995) *Am. J. Physiol.* **269,** H203–H214
49. Maruoka, N. D., Steele, D. F., Au, B. P., Dan, P., Zhang, X., Moore, E. D., and Fedida, D. (2000) *FEBS Lett.* **473,** 188–194
50. Tian, L., Chen, L., McClafferty, H., Sailer, C. A., Ruth, P., Knaus, H. G., and Shipston, M. J. (2006) *FASEB J.* **20,** 2588–2590
51. El Sayegh, T. Y., Arora, P. D., Laschinger, C. A., Lee, W., Morrison, C., Overall, C. M., Kapus, A., and McCulloch, C. A. (2004) *J. Cell Sci.* **117,** 5117–5131
52. Leonard, M., Zhang, L., Zhai, N., Cader, A., Chan, Y., Nowak, R. B., Fowler, V. M., and Menko, A. S. (2011) *Dev. Biol.* **349,** 363–377
53. Yu, D., Zhang, H., Blanpied, T. A., Smith, E., and Zhan, X. (2010) *Exp. Cell Res.* **316,** 848–858